*Pure Appl. Chem.*, Vol. 71, No. 6, pp. 1007–1017, 1999.
Printed in Great Britain.


# Pattern formation and symmetry-breaking bifurcations fueled by dissipation of chemical energy: a possible model for morphogenesis?*†

Reuben H. Simoyi

*Center for Nonlinear Science and the Chemistry Department, West Virginia University, Morgantown, WV 26506-6045, USA*

*Abstract:* A solution containing a reacting, autocatalytic and bistable chemical system can spontaneously form patterns and structure from erstwhile homogenous aqueous reaction solutions. Among some of the patterns formed are concentric rings and thermal plumes. The exothermic chemical reaction fuels the pattern-formation through a coupling of Marangoni and Rayleigh–Bénard-type thermogravitatioal effects. The thermogravitational effects arise from multicomponent convection which fuels the formation of salt fingers. These fingers later curl upwards to form thermal plumes. The concentric patterns result from the formation of a complete convective torus. The formation a series of stationary convective tori suggest that there is a possibility of other mechanisms in solution which can form Turing-like patterns.

## INTRODUCTION

The mechanism for the development of structure and form from erstwhile homogenous media has baffled scientists for years. The age-old problem of geological layering, Liesegang rings, is still searching for a solid explanation [1]. The mathematical description of symmetry-breaking bifurcations using the standard and symmetric hydrodynamics, reaction and diffusion equations requires special preconditions [2] which may be difficult to replicate in realistic physical systems.

By far, the most important advance in the field of pattern-formation and symmetry-breaking bifurcations, in general, was made in the epoch-making paper by Alan Turing in 1952 in which he proposed that a coupling of diffusion with nonlinear chemical kinetics was sufficient to produce stationary solutions which lead to spatiotemporal inhomogeneity [3]. At first glance, this coupling seems to be a perfect match for the rationalization of morphogenesis: the development of the embryo. Mathematically, the Turing mechanism can be described by the following simple equation:

$$\delta u/\delta t = D_u \nabla^2 u + F(u) \tag{1}$$

where $u$ is the vector of state variables, $D_u$ is the matrix of diffusion coefficients and $F(u)$ is the nonlinear function representing chemical kinetics. Typically, a nonlinear kinetics environment can be generated by autocatalysis or autoinhibition, especially the former [4]. Other nonlinearities can be generated by flow conditions.

A simple solution of a two-variable model of equation 1 using Dirichlet boundary conditions gives spatiotemporal patterning if the length scale of the fast-reacting activator, $[D_1/a_1]$, is shorter than that of the slow-reacting inhibitor, $[D_2/a_2]$, where $a_1$, $a_2$ are the pseudo-first-order growth rate constants [5]. Patterns should develop with a chemical wavelength, $q_0$, of:

$$q_o = \tfrac{1}{2}[a_2/D_2 - a_1/D_1]^{\frac{1}{2}} \tag{2}$$

*Lecture presented at the 7th International Chemistry Conference in Africa & 34th Convention of the South African Chemical Institute, Durban, South Africa, 6–10 July 1998, pp. 919–1024.
†Most of the experimental data reported here were obtained in collaboration with Prof. Martincigh of the University of Natal.

Physicists and chemists spent the next four decades after Turing's publication trying to design a chemical system that could generate spatiotemporal patterns based on Turing's simple mathematical scheme. It was not until 1990 that De Kepper *et al*. using a very elegant experimental setup, obtained Turing patterns using the chlorite-iodide-malonic acid chemical system (CIMA). They were able to sustain spatiotemporal inhomogeneity between two continuously stirred tank reactors (CSTR) [6].

Despite De Kepper's success, serious problems still exist in the attempt to use Turing's theory to rationalize morphogenesis. In the first instance, Turing suggested that the chemicals-like particles mentioned in his theory were 'morphogens'. No-one has yet been able to isolate these morphogens. Secondly, and most important, reaction and diffusion forces are not the only forces operating in a chemical system bifurcating to spatiotemporal patterns [7]. Convection is the most important product of reaction-diffusion forces [8]. Convection can be formed by thermal and concentration gradients which subsequently produce density gradients. It is difficult to ignore convection in a realistic chemical or biological system. De Kepper's and other subsequent Turing patterns were generated in gels which effectively suppress convection [9]. In a realistic system, how much stronger are reaction-diffusion forces than the convection they generate? In the embryonic medium, can one assume a convection-less medium as suggested by Turing's mathematical derivation?

In our ongoing research, we have taken a very highly convective system [10] and have attempted to characterize its symmetry-breaking bifurcations. We have chosen a bistable, exothermic chemical reaction medium and subjected it to a lateral instability through a perturbation generated by the addition of the autocatalyst [10]. We have examined the wave front shapes, wave velocities and the patterning generated in the wake of the wave. Our research efforts are aimed at attempting to generate Turing or Turing-like patterns in an environment that includes convection. We conjecture that the degree of spatiotemporal complexity required for morphogenesis cannot be explained from simple reaction-diffusion coupling. While zebra stripes and leopard spots can be explained from Turing-based mechanisms, development of three-dimensional structure, however, contains further complexity which is not contained in the in the basic reaction-diffusion mechanisms.

## EXPERIMENTAL

### Materials

The following analytical grade reagents were used without further purification: thiourea, 2-methylthiourea (Aldrich), perchloric acid (69–71%), methyl red, bromophenol blue, soluble starch (Fisher), barium chloride and aminoiminomethanesulfinic acid (Eastman Kodak). The commercially available technical grade sodium chlorite (Aldrich) varied in purity from 78 to 81%. A single recrystallization (ethanol-water mixture) brought the assay to 96%. The sodium chorite was collected as its dihydrate. The analysis of sodium chlorite was performed iodometrically by adding excess acidified iodide and titrating the liberated iodine against standard thiosulfate with freshly prepared starch as indicator [11]. Stock solutions of sodium chlorite were prepared fresh for each set of experiments and sometimes stabilized with 0.001 M sodium hydroxide [12].

### Methods

Different vessel shapes were used for the study of specific spatiotemporal phonomena. General experiments were carried out in Petri dishes made from Pyrex with an internal diameter of 88 mm. For the study of spatiotemporal patterns, a reaction vessel, which best represented an unbounded $x$–$y$ plane of length 24.3 cm and 15.3 cm was used. A rectangular vessel, 25.3 cm and 0.5 cm wide was used for the study of fingering patterns of the double-diffusive regime. Experiments carried out in polycarbonate, polystyrene, and polyethylene Petri dishes gave varying induction times. [13] The type of vessel material is very important in determining the induction period before the appearance of the wave front and patterns in untriggered reaction solutions (wave triggering could be electrical or chemical). Sodium chlorite, the sulfur compound, perchloric acid and indicator were thoroughly mixed before being poured into reaction vessels to depths of between 1.7 mm to 3.3 mm. The 3.3 mm depth was the upper limit for the observation of pseudo-two-dimensional patterns in the bulk solution. Deeper solutions gave more complex three-

dimensional patterns. Chlorite was always added last by means of a rapid delivery pipette. The reagents were mixed in a separate beaker and vigorously mixed for 15 s before being poured into the Pyrex Petri dish, swirled around and allowed to settle. The volume of reagents used determined the depth of the solution. Swirling the Petri dish was very important for shallow layers to ensure a uniform surface and depth. The induction period was defined as the interval between the complete delivery of the chlorite reagent and the appearance of the acid wave front. Acid-base indicators were used to monitor the progress of the reaction by following the production of $H^+$.

### Image analysis and wave dynamics

Video imaging techniques were used for studying the wave velocities, the structure of propagating wave fronts and the spatial patterns. All experiments were recorded using a PULNIX TMC 74 color camera attached to a Sony PVM-1334Q RGB monitor and a Panasonic AG-1960 professional video cassette recorder. The video cassette recorder and the RGB monitor were also interfaced to a Pentium 200 computer via a PCVision Plus frame grabber model PFGPlus-640-3-60 capable of storing a $640 \times 480$ square pixels image. The recorded experiments were played back on the video cassette and desired frames captured and stored as TIFF files. Image analysis was via Bioscan Optimas version 6.0 software. The velocities were measured using the motion analysis macro of the Bioscan software which uses Microsoft Excel 4.0 for statistical analysis.

### The chemistry of the waves

The wave is produced when unstirred solutions of a class of thiocarbonyl compounds are oxidized by chlorite [14]. The patterns then appear in the bulk solution in the wake of the lateral instability. The compounds used in this study are thiourea $(NH_2)_2\ C=S$, methylthiourea, $CH_3NH(NH_2)C=S$, and aminoiminomethanesulfinic acid, $H_2N(=NH)CSO_2H$. The general equation for the oxidation can be written as:

$$R_1R_2C=S + 2ClO_2^- + H_2O \rightarrow SO_4^{2-} + R_1R_2C=O + 2H^+ + 2Cl^- \quad \text{(R1)}$$

$R_1$ and $R_2$ are the two groups attached to the carbon atom that is bonded to the sulfur atom. These reactions show clock reaction characteristics in which initially there is a quiescent period with no activity in the reaction indicators. At the end of the induction period there is a sudden production of sulfate, chlorine dioxide, and acid [15]. The acid and sulfate are formed simultaneously from the oxidation of the sulfonic acid intermediate, $R_1R_2'CSO_3H$:

$$R_1R_2'CSO_3H + 2H_2O \rightarrow SO_4^{2-} + R_1R_2C=O + 4H^+ + 2e^- \quad \text{(R2)}$$

where $R_2'$ is of the form $-N=$ for thioureas. The chlorine dioxide, $ClO_2$, is formed by an extraneous reaction between the excess chlorite, $ClO_2^-$ and HOCl [16]:

$$2ClO_2^- + HOCl + H^+ \rightarrow 2ClO_2 + Cl^- + H_2O \quad \text{(R3)}$$

Hypochlorous acid is the autocatalytic species which controls the rates of reaction and wave propagation velocity under isothermal conditions. The mechanism for autocatalysis involves the reactive intermediate $Cl_2O_2$ which leads to quadratic autocatalysis [17,18]:

$$ClO_2^- + HOCl + H^+ \rightarrow Cl_2O_2 + H_2O \quad \text{(R4)}$$

followed by:

$$Cl_2O_2 + 2e^- + 2H^+ \rightarrow 2HOCl \quad \text{(R5)}$$

These reactions are accompanied by large heat evolution. The heat generated by the reaction is very high. For example, the reaction of thiourea and chlorite has a reaction enthalpy change in excess of $-1160$ kJ/mol [19]. Enthalpy changes for chlorite oxidation of aminoiminomethanesulfinic acid and aminomethanesulfonic acid were experimentally determined as $-880$ kJ/mol and $-630$ kJ/mol, respectively. Temperature changes at the reaction front can go as high as $T = 70\,^{\circ}C$ depending upon

initial reagent concentrations. In our study the temperature jump was restricted to 3.8 °C. Higher initial reagent concentrations gave much higher temperature jumps.

In unbuffered solutions production of $H^+$ was used as an indicator for the position of the wave front. Methyl red, methyl orange and bromophenol blue were the acid-base indicators used. Other indicators used include $BaSO_4$ precipitation (using aqueous $BaCl_2$) and freshly prepared starch. Formation of $SO_4^{2-}$ anywhere in the solution could be indicated by the formation of white $BaSO_4$ [20]. The light reflected on the $BaSO_4$ crystals can clearly indicate the direction of fluid flow at the surface and within the bulk of the solution. Formation of $ClO_2$ could be followed by the deep blue color it forms with starch indicator.

## EXPERIMENTAL RESULTS

The experimental results reported here were obtained from waves that were initiated by a 0.05-mL drop of solution containing HOCl (introduced mostly as chlorine water, $Cl_2(aq)$). Upon addition of the autocatalyst, a wave of chemical reactivity was generated which swept across the vessel from this point of initial perturbation. The wave was mostly followed by the formation of white barium sulfate precipitate. The wave started with a rapid lateral velocity. This rapid velocity was not maintained as the wave quickly decelerated to attain some constant velocity which was determined by the initial reactant concentrations (higher reagent concentrations gave higher lateral velocities). The available chemical energy seemed to be solely responsible for the wave propagation velocity. The wave velocity variations with respect to time are shown in Fig. 1. The wave velocity variation with respect to time was sigmoidal, and could be modeled by the rise in autocatalyst concentration, [HOCl], in quadratic autocatalysis. Superimposed on Fig. 1 are the types patterning observed in regions marked I to III. In region I, the wave starts slowly and quickly gathers speed.

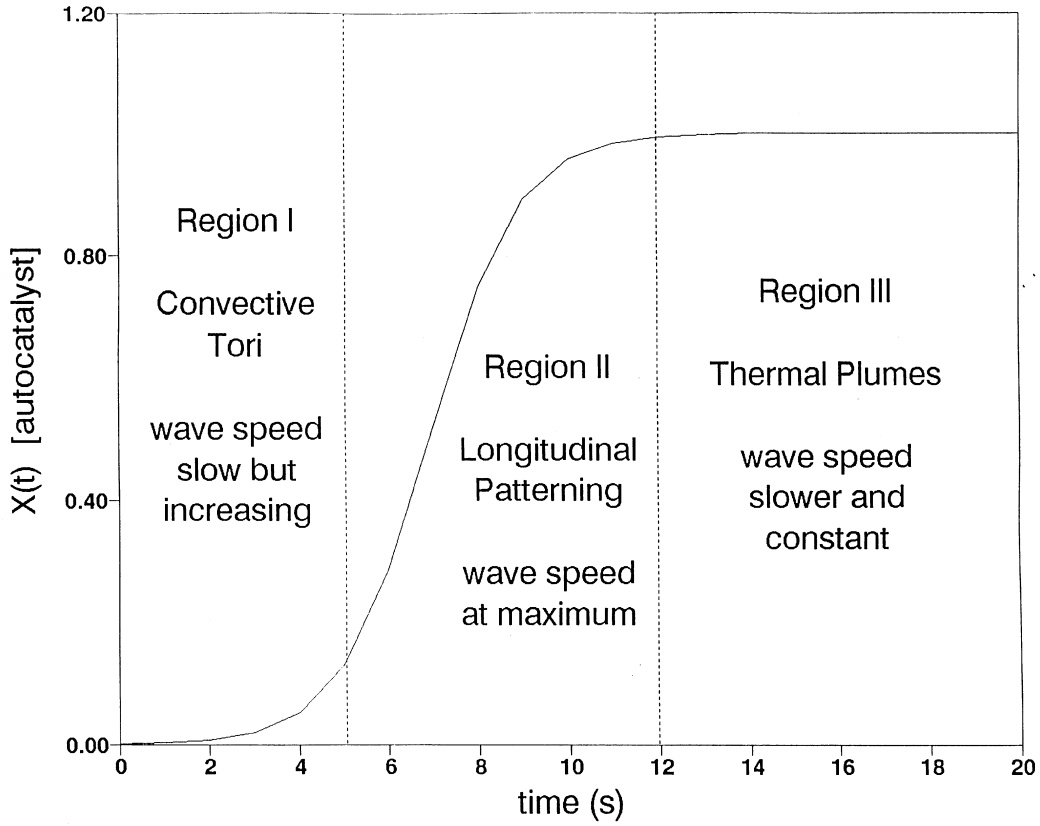


**Fig. 1** Plot of quadratic autocatalytic build-up of HOCl with respect to time for the simple reaction: $X + Y \rightarrow 2X$ where X = HOCl. Plot calculated with hypothetical concentrations of $X_0 = 0.001$ M and $Y_0 = 1.00$ M. In regions I and II the concentration of autocatalyst is proportional to the wave velocity. Coupling of Rayleigh–Bénard and thermocapillary forces is relevant in regions I and III. This coupling produces the observed organization of concentric patterning and thermal plumes, respectively.

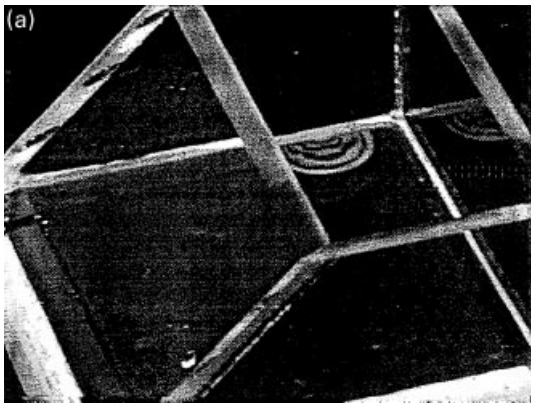


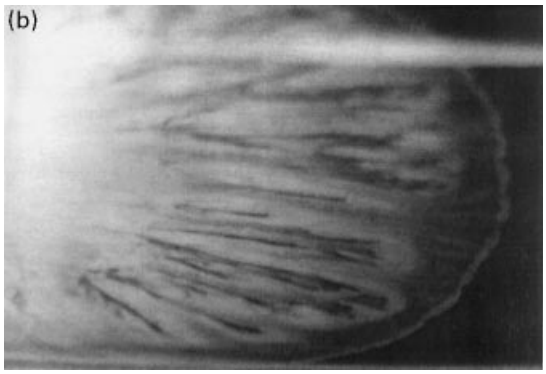


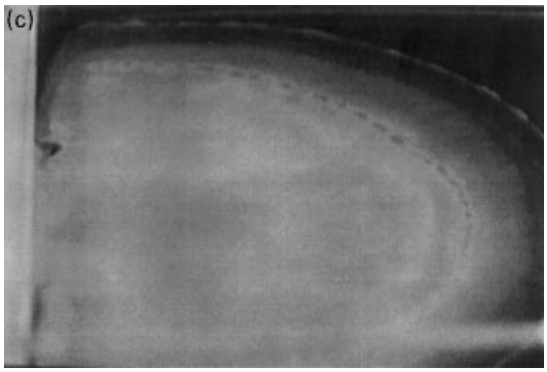


**Fig. 2** (a) Image of the concentric patterns observed in region I of Fig. 1. Four circular bands of precipitation can be seen. $[ClO_2]_0 = 0.0225$ M, $[SC(NH_2)_2]_0 = 0.0113$ M, $[BaCl_2]_0 = 0.0488$ M. (b) The longitudinal patterning observed in region II of Fig. 1. The wave velocity has increased enough to the extent that the thermocapillary convection is much stronger than the thermogravitational forces with the resulting alignment of the precipitation patterns in the direction of the wave propagation. $[ClO_2]_0 = 0.0225$ M, $[SC(NH_2)_2]_0 = 0.0113$ M, $[BaCl_2]_0 = 0.0488$ M. (c) The thermal plumes (or volcanic eruptions observed in the region III of Fig. 1.

Before the wave velocity picks up, the reaction solution shows the fascinating self-organization of concentric patterning (see Fig. 2a). The solution shows concentric rings of alternate barium sulfate precipitation and null precipitation. This type of self-organization is difficult to maintain in ungeled aqueous environments as convective instabilities are expected to annul any emerging patterns [21]. Indeed, the concentric patterns can be maintained (depending on solution depth) for about 30 s before they are annihilated.

In region II, as the wave gathers speed, the rapid horizontal motion alters the patterning from the concentric patterns to what can be called 'longitudinal patterns' (see Fig. 2b). In this region, the barium sulfate precipitate is aligned along the direction of wave propagation. Each longitudinal line of precipitation is aligned in the form of a screw motion stretched along the line of wave propagation. This is much more evident in a real-time observation of the development of the patterns. Figure 2b also shows the (by now) distorted concentric patterns at the center of the propagation pattern which represents the point of initial perturbation.

The autocatalyst concentration reaches some maximum value in region III, and the wave velocity also attains a constant value. The most interesting part of this wave is that region III contains repeating areas of violent hydrodynamic activity in the form of 'volcanic-like' eruptions. Figure 2c shows the appearance of the these eruptions which are closely related to 'thermal plumes'. Formation of plumes is periodic. Figure 3 gives a schematic sketch of the region where the thermal plumes are formed. In general, the wave always shows three distinct precipitation regions Region I (in Fig. 3) forms the leading edge of the wave front. The very leading front of the wave shows an annulus of null precipitation. After the wave front ring there is a wide region of very faint precipitation (region I). Behind this, is a region of slightly denser precipitation (region II) and finally a region of thick homogeneous precipitation (region III). The thermal plumes are formed between regions II and III. After being formed between regions II and III; they are next formed along the line dividing regions I and II. The wave front, by then will have moved on, and the ring of plumes becomes the new region II and III interface. This sequence is repeated indefinitely for as long as the vessel boundaries do not come into play. In large vessels one can observe up to 20 such sequences.

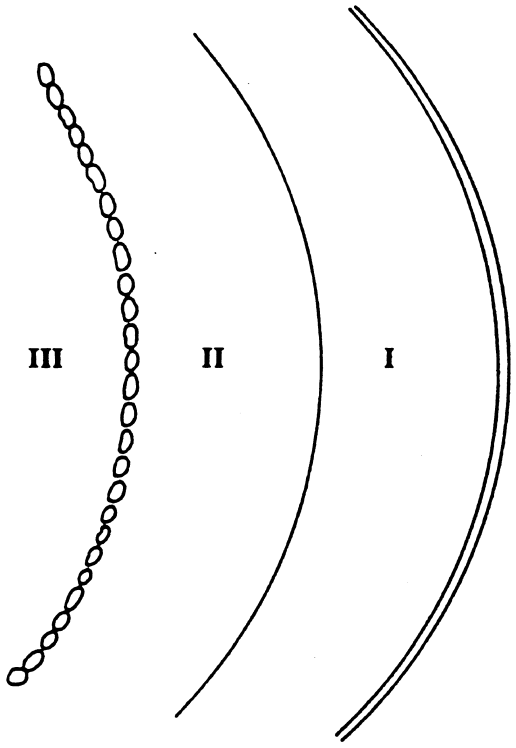


**Fig. 3** Schematic sketch of the wave front showing the regions mentioned in the text. The wave is propagating from left to right. The thin annulus of null precipitation is the leading front. Region I has light precipitation, II a little heavier, and III heaviest. The plumes are formed at the interface of regions II and III.

## DISCUSSION

In this section we are concerned primarily with the mechanism that forms the patterning observed in regions I and III of Fig. 1. Region I, especially, comes very close to the stationary solutions that characterize Turing patterns [3] (as shown in Fig. 2a). Is it possible to generate Turing-like structures in

an environment that couples convection with the standard reaction-diffusion forces? Wave propagation fueled by reaction-diffusion forces is very slow (about 20× slower) than the propagation velocity monitored in these experiments of 3–7 mm per second [13]. Hence it is safe to assume that reaction-diffusion forces will be negligible compared to convective forces in this propagation mechanism.

## Mechanism of formation of concentric patterning

The mechanism that forms these concentric patterns seen in region I of Fig. 1 (see Fig. 2a) is very important for it should be able to explain and quantify the forces that apply in ungeled aqueous environments with unchecked convection. The concentric patterns are as a result of the formation of a convective torus [21]. The formation of a complete convective roll involves alternately rising and falling regions of reaction solution. Any motion in the vertical z-axis has to result from Rayleigh–Bénard (thermogravitational) type of convection [22], while motion in the $x$-y plane results from thermocapillary convection (surface tension effects) [23]. The final convective roll is a result of the coupling between Rayleigh–Bénard (in the form of multicomponent convection) and Marangoni (thermocapillary) instabilities.

Thermocapillary forces can be estimated from the Marangoni number $Ma$ [23]:

$$Ma = -(\partial\sigma/\partial T)\Delta T \ell/\eta\chi \tag{7}$$

where $\ell$ is the length of the free surface, $\eta$ the dynamic viscosity, $\chi$ the thermal diffusivity and s is the surface tension of the reaction solution. $\partial$s/$\partial T$ is the surface tension temperature gradient. This is a negative value as surface tension normally decreases with increase in temperature. In a particular reaction solution of interest, the only variable in equation 7 will be $\Delta T$. The gravitational buoyancy forces can be deduced from the Grashof number, Gr [24]:

$$Gr = -(\partial r/\partial T)g\Delta T d^3/\eta\nu \tag{8}$$

where r is solution density, $g$ is earth's gravity, d is depth of solution and $\nu$ is kinematic viscosity. The values of $\partial$s/$\partial T$ and $\partial$r/$\partial T$ will determine the relative responses of each force (Marangoni or Rayleigh–Bénard effects, respectively) to $\Delta T$. In the chlorite-thiourea reaction we calculated $\partial$s/$\partial T$ to be $-8.6\times10^{-5}$ N/m/K and $\partial$r/$\partial T$ to be $-0.4\,\mathrm{kg/m^3/K^{1.25}}$. In our experiments the Marangoni effect is more sensitive to $\Delta T$ than the thermogravitational effect. For example for $\Delta T = 1$ °C Ma = 66 600, Gr = 170 for d = 3.3 mm and $\ell$ = 100 mm. Thus as temperature jump $\Delta T$, goes up, we expect a dominance of the thermocapillary effects over buoyancy effects, especially in laterally unbound layers.

Initially, before the reaction gathers speed (in region I of Fig. 1), both thermocapillary and buoyancy forces are comparable and couple effectively. This is the region in which convective tori are formed. As the reaction's rate, and hence $\Delta T$, increases, thermocapillary forces start to dominate and vertical buoyancy forces can no longer be effective to display any organization on this time scale. This is the region in which precipitation patterns show longitudinal patterning in the direction of wave propagation (Fig. 2b, region II of Fig. 1). As the wave slows down, the buoyancy forces start being effective once again, resulting in the volcanic-type thermal plumes behind the wave front

The chlorite-thiourea and chlorite-methylthiourea reactions are known to produce double-diffusive convection and fingering patterns [10,26]. The reaction products (inorganic salts) are heavier than the reactants (uncharged organic molecules) at isothermal conditions [10]. The formation of a convective torus involves the leading edge of the wave front (a) 'fingering' down the reactant solution (b) flowing backwards, and then (c) flowing upwards to complete the cycle (roll). All processes; a, b and c, have been observed in this and comparable chemical systems. The only requirement for the convective torus to be formed is chronological coherence of (a)→(b)→(c). Figure 4a shows how this can easily be achieved. Process (a) is basic fingering: the product solution is only lighter than the reactant solution when it is at the elevated temperature, $T_0 + \Delta T$. Loss of heat by the front will render the product solution heavier and this will force it downwards into the reactant solution. At the bottom of the reaction solution is the resident back flow which will sweep the finger backwards, thus effecting process (b). The upward motion of the plume is fueled by the acceleration of the autocatalytic reaction (which leads to a higher $\Delta T$, and hence greater buoyancy) and the availability of reactants. Figure 4b shows the experimentally observed temperature profile of a nearly fully formed convective roll which is about 2 mm wide. Although there is a sharp rise in temperature at the wave front, close examination

shows an area of chemical reactivity in which the very front tip of the wave does not give the full $\Delta T \approx 3.8\,^{\circ}C$ temperature-jump. This is important in the generation of the fingering regime. At $\Delta T < 3.8\,^{\circ}C$ the product solution is heavier than the reactant solution, thus establishing the fingering patterns. Further reaction and subsequent attainment of the full temperature-jump then renders the product solution lighter.

(a)

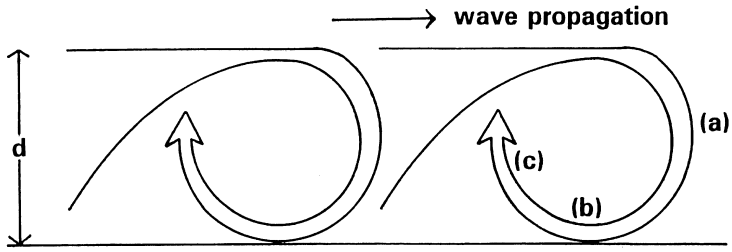


(b)

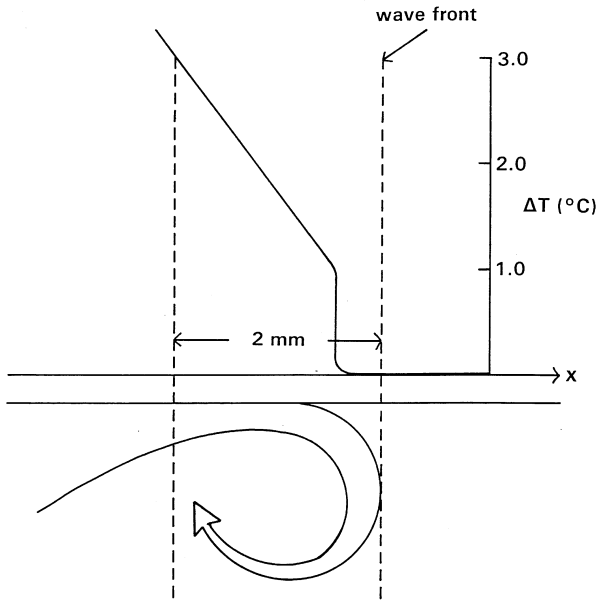


**Fig. 4** (a) Schematic diagram of the formation of a series of convective tori. The regions (a), (b) and (c) described in the text are clearly marked. (b) Temperature profile of one of the convective rolls shown in (a). The very front tip of the wave it at a lower temperature than the in the bulk of the reacted solution, and hence the ability to form fingering patterns. The lower temperature at the wave front is due to incomplete chemical reaction as well as heat loss to the colder, unreacted bulk solution.

Using standard video-imaging data, we observed that the fluid surrounding convective tori spins in the same direction: the top part spins towards the direction of wave propagation, but in between tori there was quiescence. Figure 5 shows a schematic sketch of two adjacent convective rolls in which a finger and a plume exist side-by-side. This explains the transport of $BaSO_4$ crystals from the region in-between adjacent convective rolls. Standard treatment and understanding of convective rolls suggests that a finger and a plume cannot exist side by side as shown in Fig. 5. This standard treatment applies only to stationary solutions like the Rayleigh–Bénard convection [22]. In this chemical system, the convective roll on the left is formed first while the solution now occupied by the roll on the right still contains only the reactant solution. The torus on the right is formed after the one on the left is fully formed. Continuous forward propagation (e.g. region I in Fig. 3 is moving both forward and downwards) will destroy the circular symmetry of the torus, giving a more oval shape which give rise to thermal plumes later in the wave's propagation.

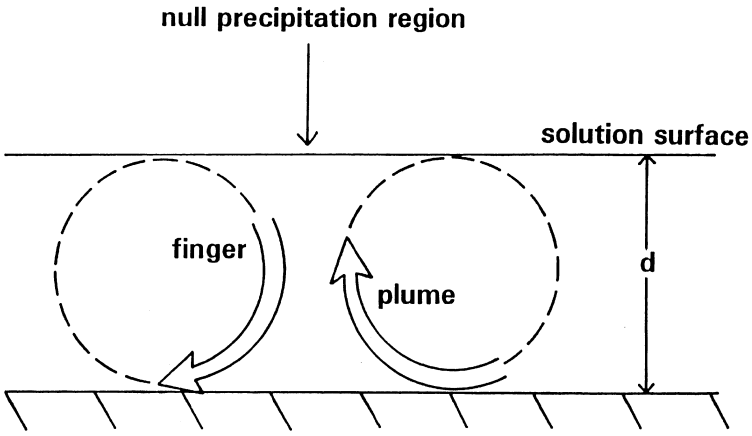


**Fig. 5** Diagram showing how two adjacent tori contain fluid moving in opposite directions although they are both spinning clockwise. Observation from the top will show banded structure of alternate precipitating regions.

## Mechanism of plume formation

The mechanism of the formation if thermal plumes is easily understood from the schematic sketches shown in Figs 6 and 7. One can imagine that as the wave slows down, one will not obtain the clear separation of convective tori as shown in Figs 2a and 5. Thus the concentric convective tori begin to overlap, with the plume of the new torus coming through the previous torus as seen in Figs 6e and 7. Figure 6 clearly shows the development of a finger which subsequently becomes the plume that forms the 'volcanic eruptions'. The leading wave front in (a) is cooled by the surrounding unreacted solution, becomes heavier and starts to sink, forming a finger (c) and (d). Near the bottom of the solution the finger is swept backwards by the resident back flow that balances the forward motion on top (d). The finger then

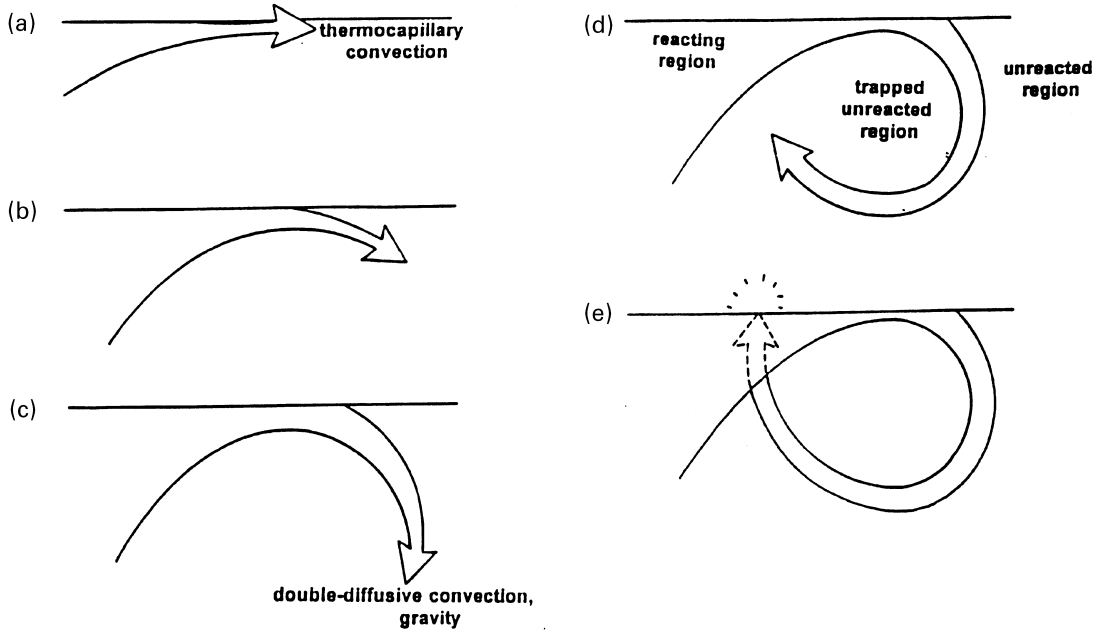


**Fig. 6** The development of a convective torus which then forms the thermal plumes. (a) Wave direction during the region of inhomogeneous precipitation. (b) The start of double-diffusive convection as the wave slows down. (c) Pronounced double-diffusive effect coupled with back flow. At this point, apart from gravitational effects, the finger will experience the return flow as seen in Fig. 6. (d) A nearly completed 'convective roll'. (e) A complete convective roll (which is in the form of a torus) which shows the formation of thermal plumes (volcanoes).

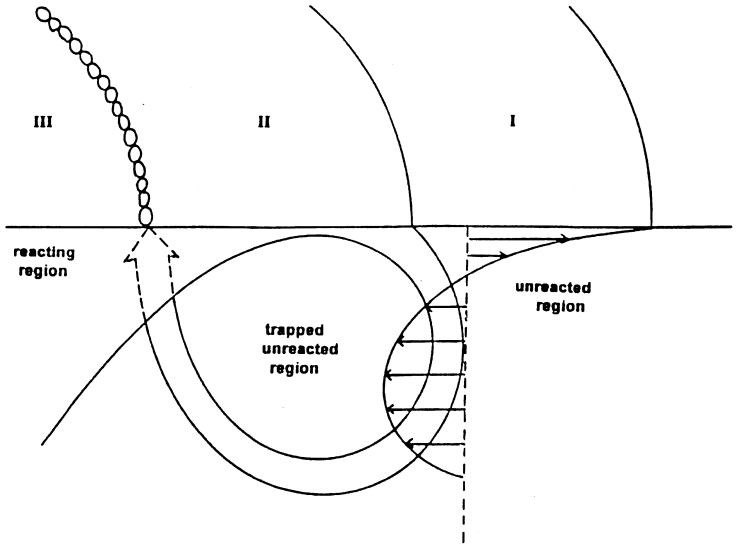


**Fig. 7** Combination of Fig. 3 and 6e which shows the positions of the relevant interfaces.

turns into a plume in (e), reaching the surface in a violent turbulent eruption. Figure 7 superimposes both Fig. 2 and 5e to further show how these plumes are formed.

## CONCLUSION

In this manuscript we have managed to show how an exothermic, bistable chemical reaction can show symmetry-breaking bifurcations from the dissipation of chemical energy. The chemical energy, derived from the exothermicity of the reaction produces surface tension and density gradients. The coupling of the resulting thermocapillary and thermogravitational effects produces coherence in the form of patterns. The concentric patterns, especially, closely mimick the Turing patterns whose existence has been based solely on a coupling of reaction and diffusion. The formation of pure hydrothermal waves from what appears like a Bénard–Marangoni [27,28] instability can fuel symmetry-breaking bifurcations. These experimental observations suggest that convection may be a very important factor in the generation of structure and form from erstwhile homogenous media.

## ACKNOWLEDGEMENTS

We acknowledge the National Science Foundation for financial support through Grant No. CHE-9632592.

## REFERENCES

1 M. C. Cross, P. C. Hohenberg. *Rev. Mod. Phys.* **65**, 851 (1995).

2 L. M. Pismen. In *Dynamics of Nonlinear Systems* (V. Hlavacek, ed.), pp. 47–84. Gordon & Breach, New York (1986).

3 A. M. Turing. *Philos. Trans. R. Soc. London B.* **37**, 37 (1952).

4 C. R. Chinake, E. Mambo, R. H. Simoyi. *J. Phys. Chem.* **98**, 2908 (1993).

5 J. D. Murray. *Mathematical Biology*. Springer-Verlag, Berlin (1989).

6 Q. Ouyang, J. Boissonade, J. C. Roux, P. De Kepper. *Phys. Lett.* **134**, 282 (1989).

7 B. S. Martincigh, R. H. Simoyi. *Phys. Rev. E* **52**, 1606 (1995).

8 D. A. Vasquez, J. W. Wilder, B. F. Edwards. *Phys. Fluids A* **4**, 2410 (1992).

9 W. Jahnke, W. E. Skaggs, A. T. Winfree. *J. Phys. Chem.* **93**, 740 (1989).

10 C. R. Chinake, R. H. Simoyi. *J. Phys. Chem.* **98**, 4012 (1994).

11 R. H. Simoyi. *J. Phys. Chem.* **89**, 3570 (1989).

12 D. M. Kern, C.-H. Kim. *J. Am. Chem. Soc.* **87**, 5309 (1965).

13 J. Masere, C. Muzimbaranda, M. Manyonda, S. Dube, R. H. Simoyi. *Int. J. Chem. Kinet.* **23**, 419 (1991).

14 C. R. Chinake, R. H. Simoyi. *J. Phys. Chem.* **97**, 11569 (1993).

15 I. R. Epstein, K. Kustin, R. H. Simoyi. *J. Phys. Chem.* **96**, 5852 (1992).

16 C. R. Chinake, E. Mambo, R. H. Simoyi. *J. Phys. Chem.* **98**, 2908 (1994).

17 H. Taube, H. Dodgen. *J. Am. Chem. Soc.* 713 330 (1949).

18 Gy. Rabai, M. Orban. *J. Phys. Chem.* **97**, 5935 (1993).

19 Barium chloride, $BaCl_2$, reacts with sulfate to produce a white precipitate of $BaSO_4$. Thus the presence of sulfate and hence the wave front could easily be detected the white precipitate formation.

20 B. S. Martincigh, M. J. B. Hauser, R. H. Simoyi. *Phys. Rev. E.* 52 (1995).

21 D. Villers, J. K. Platten. *J. Fluid Mech.* **234**, 487 (1992).

22 Lord Rayleigh. *Philos. Mag.* **32**, 529 (1916).

23 M.-J. Char, K.-T. Chiang. *J. Phys. D. Appl. Phys.* **27**, 748 (1994).

24 M. K. Smith, S. H. Davis. *J. Fluid Mech.* **132**, 145 (1983).

25 M. J. B. Hauser, R. H. Simoyi. *Chem. Phys. Lett.* **227**, 593 (1994).

26 J. S. Turner. *Annu. Rev. Fluid Mech.* **17**, 11 (1985).

27 H. Q. Yang. *Int. J. Heat Mass Transfer* **35**, 2413 (1992).

28 D. Krmpotic, G. B. Mindlin, C. Perez-Garcia. *Phys. Rev. E* **54**, 3609 (1996).